HYDROLOGICAL PROCESSES
Hydrol. Process. **24**, 3676–3688 (2010)
Published online 2 July 2010 in Wiley Online Library
(wileyonlinelibrary.com) DOI: 10.1002/hyp.7779

An analytical solution for describing the transient temperature distribution in an aquifer thermal energy storage system

Kuang-Yi Li,[1] Shaw-Yang Yang[2]* and Hund-Der Yeh[1]

[1] *Institute of Environmental Engineering, National Chiao Tung University, Hsinchu 300, Taiwan*
[2] *Department of Civil Engineering, Vanung University, Chungli 320, Taiwan*

Abstract:

A mathematical model is developed for predicting the temperature distribution in an aquifer thermal energy storage (ATES) system, which consists of a confined aquifer bounded from above and below by the rocks of different geological properties. The main transfer processes of heat include the conduction and advection in the aquifer and the conduction in the rocks. The semi-analytical solution in dimensionless form for the model is developed by Laplace transforms and its corresponding time-domain solution is evaluated by the modified Crump method. Field geothermal property data are used to simulate the temperature distribution in an ATES system. The results show that the heat transfer in the aquifer is fast and has a vast effect on the vicinity of the wellbore. However, the aquifer temperature decreases with increasing radial and vertical distances. The temperature in the aquifer may be overestimated when ignoring the effect of thermal conductivity. The temperature distribution in an ATES system depends on the vertical thermal conduction in the rocks and the horizontal advection and thermal conduction in the aquifer. The present solution is useful in designing and simulating the heat injection facility in the ATES systems. Copyright © 2010 John Wiley & Sons, Ltd.

KEY WORDS heat injection; well injection; mathematical model; Laplace transforms; modified Crump method; heat transfer

Received 22 September 2009; Accepted 30 April 2010

INTRODUCTION

Heat storage in the aquifer is a promising alternative to preserve the excess thermal energy for future demand. The aquifer thermal energy storage (ATES) and engineered geothermal system (EGS) are two techniques among various approaches to provide efficient sources of energy. Researches on the characterization of the aquifer suggest that the ATES system is technically feasible.

The concept of the ATES had been implemented to enhance the efficiency on thermal injection in comparison with other conventional sources of energy. Several studies had demonstrated the phenomenon of storing thermal energy in the aquifer through field experiments and/or theoretical predictions. Molz *et al*. (1978) performed an aquifer storage experiment to test the concept of heat storage in the aquifers and to provide data for calibration of the mathematical models describing the simultaneous transport of water and heat. Later, Molz *et al*. (1979) performed the second experiment consisting of an injection–production well during two injection–storage–production cycles. Palmer *et al*. (1992) did an experiment on thermal injection and storage in shallow unconfined aquifers and measured field data from the Canadian Forces Base Borden site. Carotenuto *et al*. (1999) presented the prototype of a geothermal converter install in a geothermal well on the island of Ischia (Italy) and also reported their experimental plant, the field tests, and the results of finite element simulations for the geothermal aquifer.

Bödvarsson and Tsang (1982) presented an analytical model to investigate the advancement of thermal front during injection of cold water into a fractured geothermal reservoir system, which has equally spaced horizontal fractures intersecting the injection well. Bödvarsson *et al*. (1982) developed a two-dimensional transient model for a fault-charged hydrothermal system when considering the effects of heat losses to the confining layers. Their model can be used to estimate the recharge rate from the fault source and the time of evolution. Chen and Reddell (1983) mentioned the studies related to the concept of ATES (Tsang *et al*., 1981; Doughty *et al*., 1982; Sauty *et al*., 1982) and the development of analytical solutions of temperature distribution for thermal injection in petroleum engineering (Rubinstein, 1959,1962; Avdonin, 1964; Thomas, 1967). They used a modified graphical technique for determining the aquifer thermal properties. They assumed that the heat transfer system was symmetrical with respect to the middle of plane of the aquifer, which has the upper and lower confining layers of uniform thicknesses. The transient and steady-state solutions were then developed by the Laplace–Carson and Laplace transforms. Ziagos and Blackwell (1986) presented a mathematical model for describing hot fluid

* Correspondence to: Shaw-Yang Yang, Department of Civil Engineering, Vanung University, Chungli 320, Taiwan. E-mail: shaoyang@vnu.edu.tw

injected into a thin aquifer below the ground surface with conductive heat transfer into the rocks both above and below the aquifer. The aquifer is infinitely extended over the horizontal domain. The ground surface has a specified temperature while the temperatures along the interface between the aquifer and the underlying and overlying rocks are variable. An approximate analytical solution was provided and compared to a numerical solution obtained from the Fourier transform. Molson *et al*. (1992) presented a three-dimensional finite element model for simulating the coupled density-dependent groundwater flow and thermal energy transport. Their model can be used to simulate low-temperature thermal transport problems. Mongelli and Pagliarulo (1997) proposed a simple model for describing the temperature distribution within an unconfined aquifer of semi-infinite thickness. They provided a method to determine the extent of the zone of influence and its magnitude for a given set of realistic thermal and hydrological parameters. Chevalier and Banton (1999a, b) applied the random walk method to study the thermal energy storage in the aquifers. The simulation results were compared with the analytical solution and the finite-difference solution. Based on the laboratory experiment and computer simulation, Nagano *et al*. (2002) investigated the influence of natural convection on forced horizontal flow in a saturated porous medium for an ATES system. Paksoy *et al*. (2004) compared the heating, ventilation, and air-conditioning (HVAC) system combined with an ATES system to a conventional air-conditioning system for a supermarket in Turkey. The result showed that the performance efficiency of the HVAC system integrated with the ATES system was almost 60% higher than that of a conventional system. Stopa and Wojnarowski (2006) investigated the front velocity of cold water injected into a geothermal reservoir. They developed an analytical solution by treating the specific heat and thermal capacity of the water–rock system as functions of temperature. Brookfield *et al*. (2009) presented a model for simulating the thermal pattern of the thermal stream loadings from both natural and anthropogenic sources. This model can be provided against a quantitative guidance towards establishing the essential conditions to maintain a healthy ecosystem.

The objective of this study was to develop a mathematical model for describing the temperature distribution in an ATES system. The present model considers that the injection well fully penetrates the confined aquifer, and hot water is injected into the aquifer bounded from above and below by the rocks of different properties and thicknesses. Heat energy is thus stored in the aquifer and partially transferred from water to rocks. An analytical solution in dimensionless form is developed by Laplace transforms and its corresponding time-domain solution is evaluated by the modified Crump method (de Hoog *et al*., 1982). The present solution is useful in simulating the temperature distributions in an ATES system and assessing the influences of geological properties on temperature distribution. In addition, the solution can also be used as a preliminary tool in designing an ATES system.

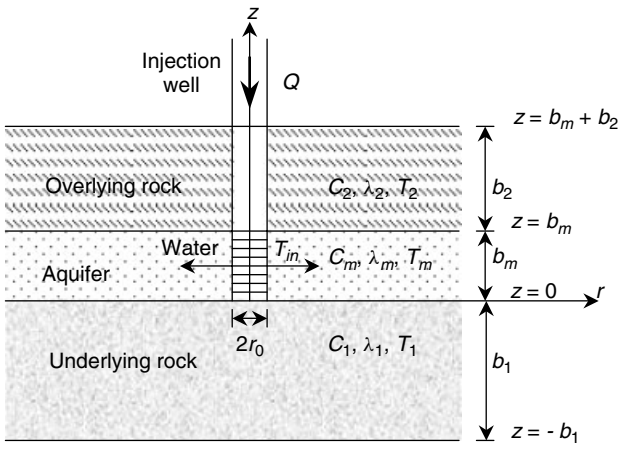

Figure 1. Schematic representation of an ATES system

ANALYTICAL STUDY

Mathematical model

A mathematical model is developed herein to simulate the transient temperature distribution in an ATES system. Hot water is injected into a fully penetrating well in an aquifer bounded from above and below by the rocks of different geological properties. Heat energy is therefore transferred from water to rocks and stored in the aquifer and rocks. The schematic representation of heat injection in an ATES system is illustrated in Figure 1. The assumptions for the model are as follows:

1. The confined aquifer is homogeneous, anisotropic, and infinite in the horizontal extent and of a uniform thickness, b_m. Heat transfer processes include the horizontal advection and thermal conduction along the flow direction in the aquifer. For the strongly anisotropic aquifer, the horizontal permeability is much larger than the vertical permeability. In addition, the densities of the water and soil media are kept unchanged, and the buoyancy flow is therefore negligible. The vertical flow and thermal conduction perpendicular to the aquifer are neglected.
2. The underlying and overlying rocks are homogeneous, anisotropic, impermeable, and of uniform thicknesses b_1 and b_2, respectively. The heat fluxes in the rocks are mainly due to the heat gradient between the aquifer and the rocks. Therefore, the horizontal thermal conduction of the rocks is negligible.
3. The injection well fully penetrates the confined aquifer and the injection rate Q is fixed.
4. The physical parameters and thermal properties of the aquifer and the underlying and overlying rocks are spatially and temporally invariant. The assumption is applicable when the changes of temperatures in the

rocks and water flow are not very large (Stopa and Wojnarowski, 2006).

5. The thermal capacity, denoted as ρc (product of density and specific heat), is a volumetric average of water and soil media. The aquifer porosity, n, represents the fraction of volume occupied by the pore space. The thermal capacity of the aquifer is thus expressed as $(\rho c)_{\mathrm{m}} = n(\rho c)_{\mathrm{water}} + (1-n)(\rho c)_{\mathrm{soil}}$.
6. The initial temperature is constant over the whole aquifer. Neglecting heat loss, the temperature of injection water, T_{in}, keeps constant all the time. In addition, the temperature in the aquifer is considered well mixed over entire thickness.
7. Before the injection, the temperatures in both rocks are uniformly distributed over vertical depth. Consider that the outer boundaries of the underlying and overlying rocks are high-permeability layers where the regional flow enables constant temperatures.

Governing equations, initial and boundary conditions

Based on the above assumptions, the equation for describing temperature distribution in the aquifer can be written as follows (Özisik, 1993, p. 25):

$$b_{\mathrm{m}}\left\{C_{\mathrm{m}}\left[\frac{\partial T_{\mathrm{m}}(r,t)}{\partial t}+v\frac{\partial T_{\mathrm{m}}(r,t)}{\partial r}\right]-\lambda_{\mathrm{m}}\left[\frac{\partial^2 T_{\mathrm{m}}(r,t)}{\partial r^2}+\frac{1}{r}\frac{\partial T_{\mathrm{m}}(r,t)}{\partial r}\right]\right\} = -\lambda_1\frac{\partial T_1(r,z,t)}{\partial z}\bigg|+\lambda_2\frac{\partial T_2(r,z,t)}{\partial z}\bigg|_{z=b_{\mathrm{m}}} \quad (1)$$

where the subscripts m, 1, and 2 denote the aquifer, underlying rock, and overlying rock, respectively; T is the temperature; λ is the thermal conductivity; b is the thickness; C is the thermal capacity; z is the vertical distance along the injection well; r is the radial distance from the centre of the injection well; and t is the time. The volumetric flux per unit area in the aquifer, i.e. flow velocity v, is $Q/(2\pi r n b_{\mathrm{m}})$.

The initial temperature of the aquifer is assumed constant, that is

$$T_{\mathrm{m}}(r,0) = T_{m0} \quad (2)$$

where T_{m0} is the initial temperature of the aquifer.

The boundary conditions at the wellbore, $r = r_0$, and infinite radial extend, $r = \infty$, are respectively

$$T_{\mathrm{m}}(r_0,t) = T_{\mathrm{in}} \quad (3)$$

and

$$T_{\mathrm{m}}(\infty,t) = T_{m0} \quad (4)$$

where T_{in} is the temperature of the injection water and T_{m0} is the initial temperature of the aquifer.

For the underlying rock, the heat conduction equation can be written as

$$\frac{\partial^2 T_1(r,z,t)}{\partial z^2} = \frac{C_1}{\lambda_1}\frac{\partial T_1(r,z,t)}{\partial t} \quad (5)$$

Neglecting the geothermal gradient, the initial condition for the underlying rock is

$$T_1(r,z,0) = T_{10} \quad (6)$$

where T_{10} is the initial temperature.

The boundary conditions for the underlying rock are

$$T_1(r,0,t) = T_{\mathrm{m}}(r,t) \text{ at the upper boundary} \quad (7)$$

and

$$T_1(r,-b_1,t) = T_{10} \text{ at the lower boundary} \quad (8)$$

For the overlying rock, the heat conduction equation can be written as

$$\frac{\partial^2 T_2(r,z,t)}{\partial z^2} = \frac{C_2}{\lambda_2}\frac{\partial T_2(r,z,t)}{\partial t} \quad (9)$$

The initial condition for the overlying rock is

$$T_2(r,z,0) = T_{20} \quad (10)$$

where T_{20} is the initial temperature.

The boundary conditions for the overlying rock are

$$T_2(r,b_{\mathrm{m}},t) = T_{\mathrm{m}}(r,t) \text{ at the lower boundary} \quad (11)$$

and

$$T_2(r,b_{\mathrm{m}}+b_2,t) = T_{20} \text{ at the upper boundary} \quad (12)$$

Semi-analytical solutions

The normalized parameters are defined as

$$T_{\mathrm{mD}}(R,\tau) = \frac{T_{\mathrm{m}}(r,t)-T_{m0}}{T_{\mathrm{in}}-T_{m0}},\ T_{1\mathrm{D}}(R,Z_1,\tau) = \frac{T_1(r,z,t)-T_{m0}}{T_{\mathrm{in}}-T_{m0}},$$

$$T_{2\mathrm{D}}(R,Z_2,\tau) = \frac{T_2(r,z,t)-T_{m0}}{T_{\mathrm{in}}-T_{m0}},\ T'_{1\mathrm{D}}(R,Z_1,\tau) = T_{1\mathrm{D}}(R,Z_1,\tau) - T_{10\mathrm{D}},\ T_{10\mathrm{D}} = \frac{T_{10}-T_{m0}}{T_{\mathrm{in}}-T_{m0}},$$

$$T'_{2\mathrm{D}}(R,Z_2,\tau) = T_{2\mathrm{D}}(R,Z_2,\tau) - T_{20\mathrm{D}},\ T_{20\mathrm{D}} = \frac{T_{20}-T_{m0}}{T_{\mathrm{in}}-T_{m0}},\ R = \frac{2r}{b_{\mathrm{m}}},\ R_0 = \frac{2r_0}{b_{\mathrm{m}}},\ Z_1 = -\frac{4z}{b_{\mathrm{m}}},$$

$$Z_2 = \frac{4(z-b_{\mathrm{m}})}{b_{\mathrm{m}}},\ B_1 = \frac{b_1}{b_{\mathrm{m}}},\ B_2 = \frac{b_2}{b_{\mathrm{m}}},\ \lambda_{1\mathrm{D}} = \frac{\lambda_1}{\lambda_{\mathrm{m}}},\ \lambda_{2\mathrm{D}} = \frac{\lambda_2}{\lambda_{\mathrm{m}}},\ \alpha_{\mathrm{m}} = \frac{\lambda_{\mathrm{m}}}{C_{\mathrm{m}}},\ \alpha_1 = \frac{\lambda_1}{C_1},$$

$$\alpha_2 = \frac{\lambda_2}{C_2},\ \alpha_{1\mathrm{D}} = \frac{4\alpha_1}{\alpha_{\mathrm{m}}},\ \alpha_{2\mathrm{D}} = \frac{4\alpha_2}{\alpha_{\mathrm{m}}},\ w = \frac{Q}{4\pi n b_{\mathrm{m}}\alpha_{\mathrm{m}}},\ \tau = \frac{4\alpha_{\mathrm{m}}t}{{b_{\mathrm{m}}}^2} \quad (13)$$

Based on Equation (13), Equations (1)–(12) can be expressed in dimensionless forms. The detailed development of the Laplace domain solution for dimensionless

aquifer temperature, $\overline{T}_{\mathrm{mD}}(R,\ p)$, is given in Appendix A and the result is

$$\overline{T}_{\mathrm{mD}}(R,\ p) = \frac{1}{p}\left(\frac{R}{R_0}\right)^{\mathrm{w}}\left[\frac{K_{\mathrm{w}}(\sqrt{A(p)}R)}{K_{\mathrm{w}}(\sqrt{A(p)}R_0)}\right]\left[1+\frac{B(p)}{A(p)}\right]-\frac{B(p)}{pA(p)} \tag{14}$$

with

$$A(p) = p + \lambda_{1\mathrm{D}}q_1\coth(4q_1B_1) + \lambda_{2\mathrm{D}}q_2\coth(4q_2B_2) \tag{15}$$

and

$$B(p) = -\lambda_{1\mathrm{D}}q_1T_{10\mathrm{D}}\coth(4q_1B_1) - \lambda_{2\mathrm{D}}q_2T_{20\mathrm{D}}\coth(4q_2B_2) \tag{16}$$

where p is the Laplace variable (Spiegel, 1965); $K_{\mathrm{w}}(\cdot)$ is the modified Bessel function of the second kind with order w; $q_i^2 = p/\alpha_{i\mathrm{D}}$, $i = 1$ and 2. In addition, the Laplace domain solutions for dimensionless temperature distribution in the underlying and overlying rocks are, respectively,

$$\overline{T}_{1\mathrm{D}}(R, Z_1,\ p) = \frac{\sinh[q_1(4B_1 - Z_1)]}{\sinh(4q_1B_1)}\left(\overline{T}_{\mathrm{mD}}(R,\ p) - \frac{T_{10\mathrm{D}}}{p}\right) + \frac{T_{10\mathrm{D}}}{p} \tag{17}$$

and

$$\overline{T}_{2\mathrm{D}}(R, Z_2,\ p) = \frac{\sinh[q_2(4B_2 - Z_2)]}{\sinh(4q_2B_2)}\left(\overline{T}_{\mathrm{mD}}(R,\ p) - \frac{T_{20\mathrm{D}}}{p}\right) + \frac{T_{20\mathrm{D}}}{p} \tag{18}$$

Simplified solutions

When the initial temperature in an ATES system is uniform, that is, $T_{m0} = T_{10} = T_{20}$, the dimensionless parameters of $T_{10\mathrm{D}}$, $T_{20\mathrm{D}}$, and $B(p)$ are equal to zero. The Laplace domain solutions of Equations (14), (17), and (18) are, respectively, reduced to

$$\overline{T}_{\mathrm{mD}}(R,\ p) = \frac{1}{p}\left(\frac{R}{R_0}\right)^{\mathrm{w}}\left[\frac{K_{\mathrm{w}}(\sqrt{A(p)}R)}{K_{\mathrm{w}}(\sqrt{A(p)}R_0)}\right] \tag{19}$$

$$\overline{T}_{1\mathrm{D}}(R, Z_1,\ p) = \frac{\sinh[q_1(4B_1 - Z_1)]}{\sinh(4q_1B_1)}\overline{T}_{\mathrm{mD}}(R,\ p) \tag{20}$$

and

$$\overline{T}_{2\mathrm{D}}(R, Z_2,\ p) = \frac{\sinh[q_2(4B_2 - Z_2)]}{\sinh(4q_2B_2)}\overline{T}_{\mathrm{mD}}(R,\ p) \tag{21}$$

If the underlying and overlying rocks are of the same geological properties and vertical thickness, then $T_1 = T_2 = T_R$, $-Z_1 = Z_2 = Z_R$, $\alpha_1 = \alpha_2 = \lambda_R/C_R$, $q_1 = q_2 = q_R$, $B_1 = B_2 = B_R$, $\lambda_1 = \lambda_2 = \lambda_R$, and $\lambda_{1\mathrm{D}} = \lambda_{2\mathrm{D}} = \lambda_{\mathrm{RD}}$. Defining $A^*(p) = p + 2\lambda_{\mathrm{RD}}q_R\coth(4q_RB_R)$, the dimensionless aquifer temperature becomes

$$\overline{T}^*_{\mathrm{mD}}(R,\ p) = \frac{1}{p}\left(\frac{R}{R_0}\right)^{\mathrm{w}}\left[\frac{K_{\mathrm{w}}(\sqrt{A^*(p)}R)}{K_{\mathrm{w}}(\sqrt{A^*(p)}R_0)}\right] \tag{22}$$

and the dimensionless rock temperature obtained from Equations (20) and (21) can be reduced to

$$\overline{T}^*_{\mathrm{RD}}(R, Z_R,\ p) = \frac{\sinh[q_R(4B_R - Z_R)]}{\sinh(4q_RB_R)}\overline{T}^*_{\mathrm{mD}}(R,\ \ p) \tag{23}$$

If the radius of the injection well is negligible, i.e. $r_0 \to 0$, then Equation (22) reduces to

$$\overline{T}^*_{\mathrm{mD}}(R,\ p) = \frac{2^{1-w}R^w}{p\Gamma(\mathrm{w})}\left[\sqrt{A^*(p)}^{w}K_{\mathrm{w}}(\sqrt{A^*(p)}R)\right] \tag{24}$$

which is identical to the equation presented in Chen and Reddell (1983), Equation (A22) if the well radius is infinitesimal, and the initial temperature and rock thickness are the same. Note that detailed development of Equation (24) is given in Appendix B.

Steady-state solution

A steady-state solution can be obtained if thermal energy loss from aquifer into rocks at any distance r is zero. In this case, thermal energy loss is only a function of r in an ATES system. Thermal energy loss from water within the aquifer must be balanced by the loss of temperature with increasing radial distance along the aquifer (Ziagos and Blackwell, 1986). Furthermore, the steady-state solutions of Equations (14), (17), and (18) are developed by applying the final-value theorem (Spiegel, 1965). The detailed development of the steady-state solution for temperature distribution in the aquifer is shown in Appendix C and the result is

$$T_{\mathrm{mD}}(R, \infty) = \left(\frac{R}{R_0}\right)^{\mathrm{w}}\left[\frac{K_{\mathrm{w}}\left(\sqrt{\frac{\lambda_{1\mathrm{D}}}{4B_1} + \frac{\lambda_{2\mathrm{D}}}{4B_2}}R\right)}{K_{\mathrm{w}}\left(\sqrt{\frac{\lambda_{1\mathrm{D}}}{4B_1} + \frac{\lambda_{2\mathrm{D}}}{4B_2}}R_0\right)}\right]\left(1 - \frac{\lambda_{1\mathrm{D}}T_{10\mathrm{D}}B_2 + \lambda_{2\mathrm{D}}T_{20\mathrm{D}}B_1}{\lambda_{1\mathrm{D}}B_2 + \lambda_{2\mathrm{D}}B_1}\right) + \frac{\lambda_{1\mathrm{D}}T_{10\mathrm{D}}B_2 + \lambda_{2\mathrm{D}}T_{20\mathrm{D}}B_1}{\lambda_{1\mathrm{D}}B_2 + \lambda_{2\mathrm{D}}B_1} \tag{25}$$

Similarly, the steady-state solutions for the underlying and overlying rocks developed from Equations (17) and (18) are, respectively,

$$T_{1\mathrm{D}}(R, Z_1, \infty) = \left(\frac{4B_1 - Z_1}{4B_1}\right)T_{\mathrm{mD}}(R, \infty) + \frac{Z_1}{4B_1}T_{10\mathrm{D}} \tag{26}$$

and

$$T_{2\mathrm{D}}(R, Z_2, \infty) = \left(\frac{4B_2 - Z_2}{4B_2}\right)T_{\mathrm{mD}}(R, \infty) + \frac{Z_2}{4B_2}T_{20\mathrm{D}} \tag{27}$$

NUMERICAL EVALUATIONS

Equations (14), (17), and (18) are expressed in terms of hyperbolic cotangent and Bessel function $K_w(\cdot)$ and their time-domain solutions may not be tractable. Therefore, the numerical routine DINLAP of IMSL (2003) developed based on a numerical algorithm originally proposed by Crump (1976) and modified by de Hoog *et al*. (1982) is adopted. This algorithm approximates Laplace inversion by expressing the inverted function in a Fourier series and accelerates the evaluation by the Shanks method (Shanks, 1955; Yeh and Yang, 2006). Equations (14), (17), and (18) are numerically inverted by this routine with the accuracy of the fourth significant digit.

Note that the Laplace domain solutions of Equations (14), (17), and (18) include Bessel function $K_w(z)$ of order w, which is non-integer and depends on dimensionless advection parameter, $Q/4\pi n b_m \alpha_m$. Using the asymptotic expansion for a large argument, $K_w(z)$ is expressed as (Abramowitz and Stegun, 1964, p. 378)

$$K_w(z) = \sqrt{\frac{\pi}{2z}} e^{-z} \left\{ 1 + \frac{\mu - 1}{8z} + \frac{(\mu - 1)(\mu - 9)}{2!(8z)^2} + \frac{(\mu - 1)(\mu - 9)(\mu - 25)}{3!(8z)^3} + \cdots \right\}, \quad \left(|\arg\ z| < \frac{3}{2}\pi \right) \tag{28}$$

where $\mu = 4\ w^2$. The evaluation of an infinite sum on the right-hand side of Equation (28) can be accelerated using the Shanks method. This method had been successfully applied to evaluate the analytical solutions for heat transfer problems (Yang and Yeh, 2008, 2009a, b).

RESULTS AND DISCUSSION

Consider that the well radius, r_0, is 0·05 m and the injection rate, Q, is 10^{-4} m^3/s. The thickness of the aquifer, b_m, is 20 m and the thicknesses of the underlying and overlying rocks, b_1 and b_2, are 50 m and 30 m, respectively. Hot water at a constant temperature of 70 °C is injected into the confined aquifer, which has an initial temperature of 20 °C. Of particular interest, the outer boundary temperatures of the underlying and overlying rocks, T_{10} and T_{20} have the fixed temperatures of 21 °C and 19 °C, respectively. They are surrounded by the high-permeability fractured layers in the regional flow or by the atmosphere in the outer boundary of the overlying rock. The parameters and geothermal properties of the aquifer and rocks given by Bödvarsson and Tsang (1982) are listed in Table I and chosen to examine the performance of the present model. The temperature versus radial distance for the aquifer is plotted in Figure 2. Figure 2a shows that the aquifer temperature increases with injection time and decreases with increasing radial distance. In addition, the aquifer temperature approaches the initial temperature at large radial distance. The figure also shows that the aquifer temperature of the large time case (say, $t = 10^5$ day) agrees with that of the steady-state solution and no advective heat transfer occurs in an ATES system when the injection time is very large. Figure 2b shows the aquifer temperature distributions in two cases with different rock thicknesses. The solid line represents the case 1 with $b_1 = 50$ m and $b_2 = 30$ m, while the dotted line denotes the case 2 with $b_1 = 50$ m and $b_2 = 5$ m for $t = 10^2$, 10^3 days, and the steady-state solution. The figure shows that the aquifer temperature in case 1 is higher than that in case 2, indicating that the rock thickness has an influence on the aquifer temperature. In fact, such an influence is mainly arisen from the effect of the upper boundary, which has a fixed and low temperature. In addition, the figure also shows that the temperatures in both the cases increase with injection time at the same radial distance.

The curves of temperature versus radial distance and vertical depth for the aquifer and rocks are shown in Figure 3. The radius of influence is considered as the distance from injection well to the location where the temperature is increased 0·5 °C to the initial temperature. Figure 3a indicates that the radii of influence are about 4·2 m for the aquifer (in the horizontal direction) and 2·9 and 23 m for the underlying and overlying rocks (in the vertical direction), respectively, at $t = 10$ day. Figure 3b shows that the radii of influence are about 12·5 m for the aquifer and 8 and 29 m for the underlying and overlying rocks, respectively, at $t = 100$ day. The figure also shows that the aquifer temperature distribution strongly depends on the injection time, especially near the wellbore. In addition, heat transfers in the underlying and overlying rocks have influence only over small distances from the injection well. The results demonstrate that the development of thermal field depends on the horizontal

Table I. Parameters used in the present model

Parameter name	Symbol	Value
Thickness of the aquifer	b_m	20 m
Thickness of the rocks	b_1, b_2	50, 30 m
Volumetric thermal capacity of the aquifer	C_m	$2{\cdot}695 \times 10^6$ J/m$^3\cdot$°C
Volumetric thermal capacity of the underlying rock	C_1	$2{\cdot}5 \times 10^6$ J/m$^3\cdot$°C
Volumetric thermal capacity of the overlying rock	C_2	$2{\cdot}65 \times 10^6$ J/m$^3\cdot$°C
Thermal conductivity of the aquifer	λ_m	2·4 W/m·°C
Thermal conductivity of the rocks	λ_1, λ_2	1·5, 2·0 W/m·°C
The aquifer porosity	n	0·3

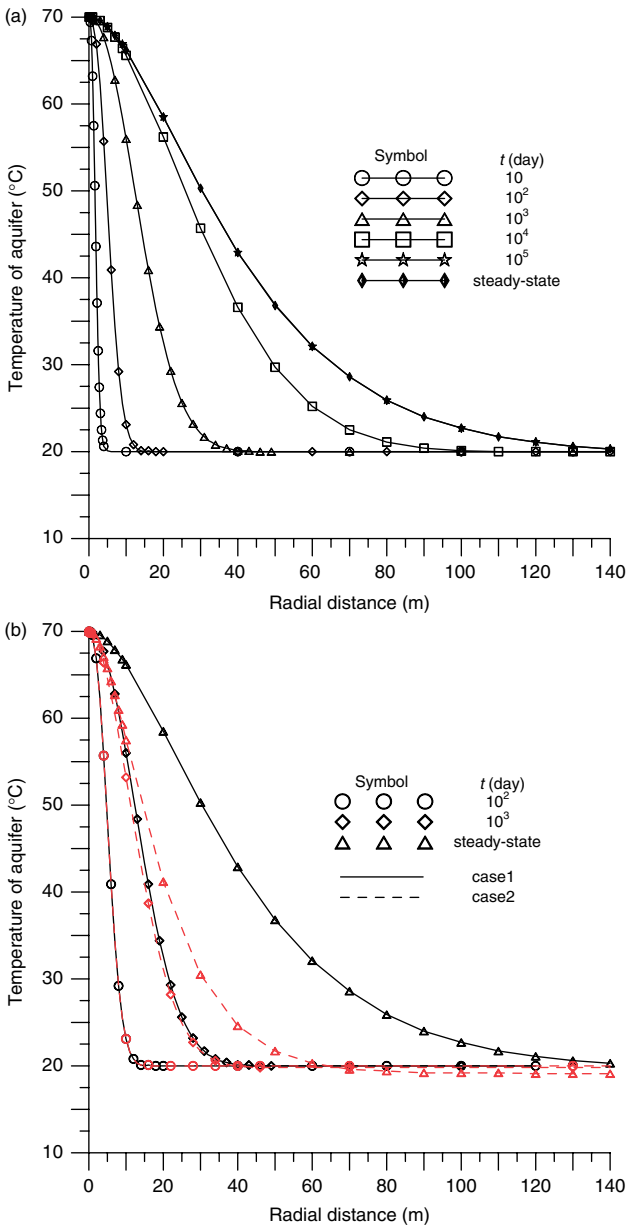

Figure 2. Plots of aquifer temperature T_m versus radial distance r for $C_m = 2{\cdot}695 \times 10^6$ J/m$^3\cdot$°C, $\lambda_m = 2{\cdot}4$ W/m·°C, $b_m = 20$ m, $T_{in} = 70$ °C, $T_{m0} = 20$ °C, and $Q = 10^{-4}$ m^3/s in an ATES system (a) for $b_1 = 50$ m and $b_2 = 30$ m (case 1) when $t = 10$, 10^2, 10^3, 10^4, 10^5 (large time) days, and the steady-state solution; (b) for $b_1 = 50$ m and $b_2 = 5$ m (case 2) when $t = 10^2$, 10^3 days, and the steady-state solution in comparison with the case 1

advection and thermal conduction in the aquifer and the vertical thermal conduction in the rocks. With the physical parameters given in Table I, Figure 4 shows the evolution of temperature profile in an ATES system at $r = 1$ m. This figure exhibits that the temperature profiles of the aquifer and rocks increase with injection time and reach steady state when the injection time is 10^5 day. It also shows that the temperature changes quickly in the aquifer and tardily in the rocks. The changes of temperature in the rocks are significant only near the injection well at early time, increase with injection time, and tend to be a linear function between the vertical distance and the temperature at large time. The result indicates that the temperature in the aquifer approaches a constant value at very large time. In addition, the temperatures in the rocks are inversely proportional to vertical distance.

The profiles of aquifer temperature versus radial distance estimated by Chen and Reddell's solution (1983) (hereinafter is referred to as the CRS) and the present solution for $T_{in} = 70$ °C, $Q = 10^{-4}$ m^3/s, $T_{m0} = 20$ °C, $T_{10} = 21$ °C, and $T_{20} = 19$ °C are shown in Figure 5. The underlying and overlying rocks are assumed to have the same physical properties, and the parameters of the aquifer and rocks are listed in Table II. The figure shows the curves of temperature versus radial distance when the injection time $t = 1$, 10, or 30 days. The dotted and solid lines denote the semi-analytical results of aquifer temperature estimated by the CRS and the present solution, respectively. Note that the CRS neglects the wellbore radius and aquifer porosity. The figure shows that the difference in transient aquifer temperature between the CRS and the present solution is not noticeable at $r \geq 0{\cdot}9$ m when $t = 1$ day, $r \geq 3$ m when $t = 10$ day, and $r \geq 4$ m when $t = 30$ day. In addition, the difference in aquifer temperature between the CRS and the present solution at large time is larger than that at small time. The present solution is of excellent prediction on aquifer temperature distribution over the range of injection time and at any radial distance. This result demonstrates that the temperature distribution of the aquifer may be underestimated if the radius of the wellbore is ignored in an ATES system.

To assess the effect of thermal conductivity λ_m on the aquifer temperature, the profile of aquifer temperature versus radial distance in an ATES system is shown in Figure 6, where hot water with a constant injection rate of $Q = 10^{-4}$ m^3/s is injected into the aquifer with the initial temperature of 33 °C. The dotted and solid lines denote the aquifer temperatures for the cases of $\lambda_m = 1{\cdot}0$ and $2{\cdot}4$ W/m·°C, respectively. The aquifer temperature decreases quickly with increasing radial distance at a fixed injection time and increases rapidly with injection time at a small radial distance and then approaches a constant value at 11 and 33 m as $t = 100$ and 1000 day, respectively, for $\lambda_m = 1{\cdot}0$ W/m·°C and at 14 and 40 m as $t = 100$ and 1000 day, respectively, for $\lambda_m = 2{\cdot}4$ W/m·°C. In addition, the aquifer temperature with $\lambda_m = 1{\cdot}0$ W/m·°C is greater than that with $\lambda_m = 2{\cdot}4$ W/m·°C under the specific radial distance and time. This result indicates that thermal conductivity parameter is crucial in affecting aquifer temperature distribution. Note that when the injection time approaches infinity, the aquifer temperature is lower than its initial temperature of 33 °C at $r \geq 130$ m for $\lambda_m = 1{\cdot}0$ W/m·°C and at $r \geq 150$ m for $\lambda_m = 2{\cdot}4$ W/m·°C. This result reflects that the impact of boundary effect on the aquifer temperature distribution. These analyses indicate that thermal conductivity plays an important role in a porous medium. An ATES system with a smaller thermal diffusivity has more efficiency than that with a higher thermal diffusivity.

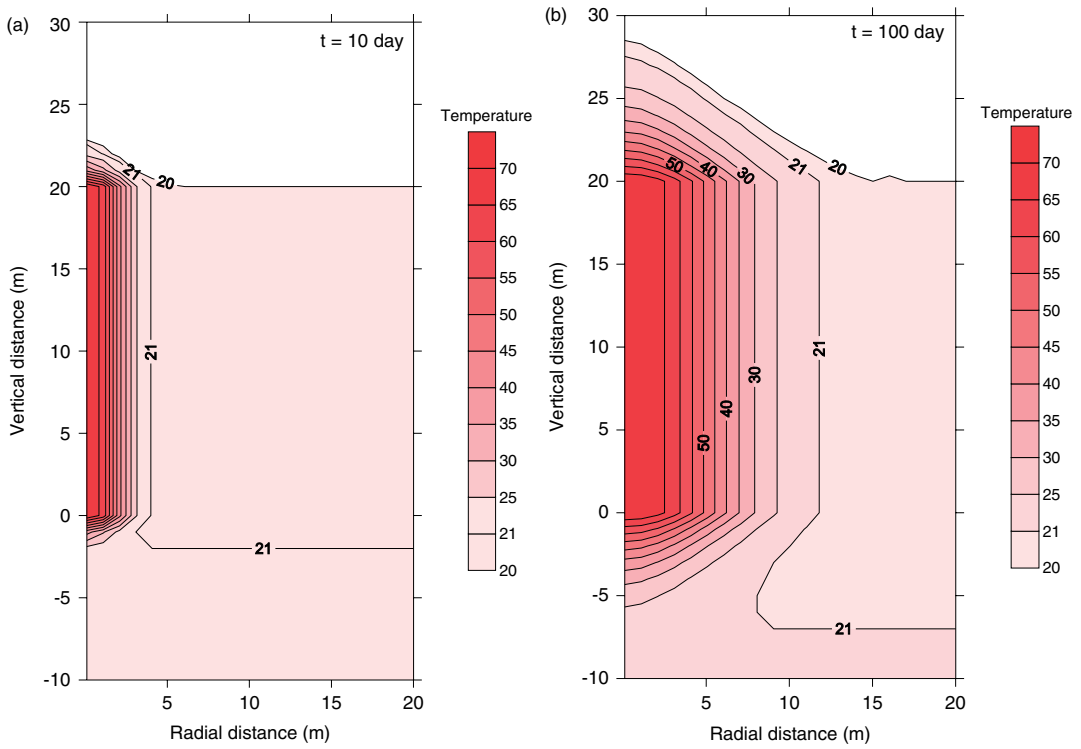

Figure 3. Plots of the isotherm of the aquifer and rocks versus radial distance r and vertical distance z when (a) $t = 10$ day and (b) $t = 100$ day

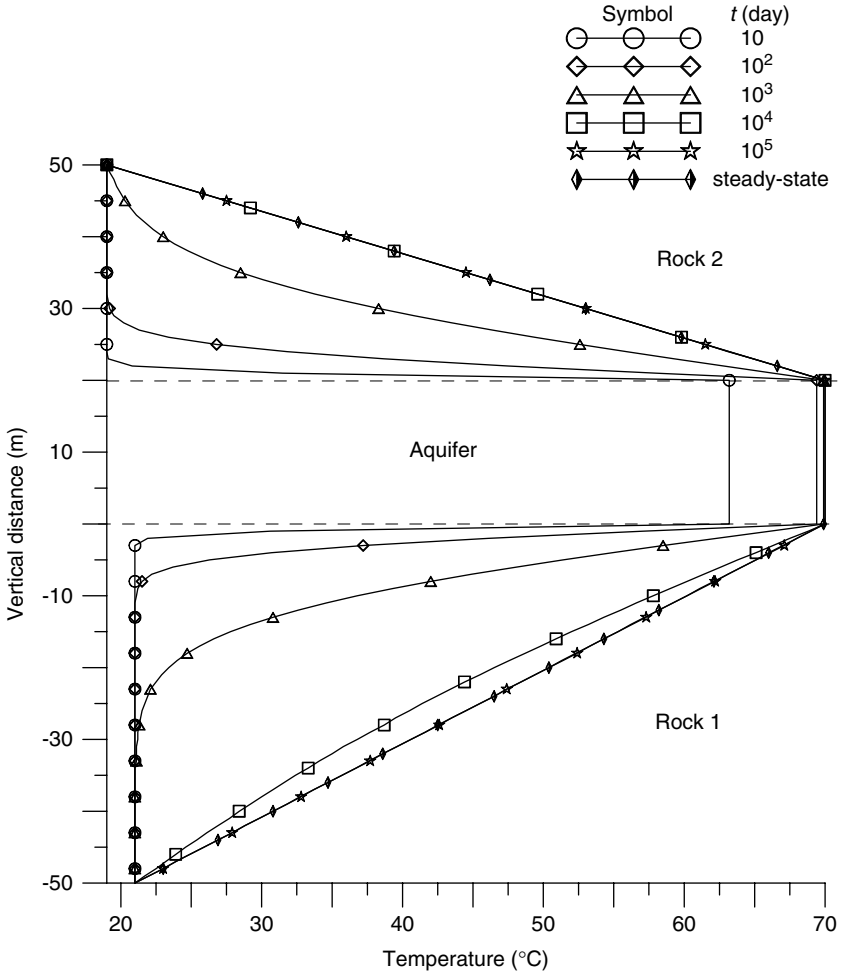

Figure 4. Plots of the isotherm of the aquifer and rocks versus vertical distance z at $r = 1$ m when the injection time $t = 10$, 10^2, 10^3, 10^4, 10^5 (large time) days, and the steady-state solution

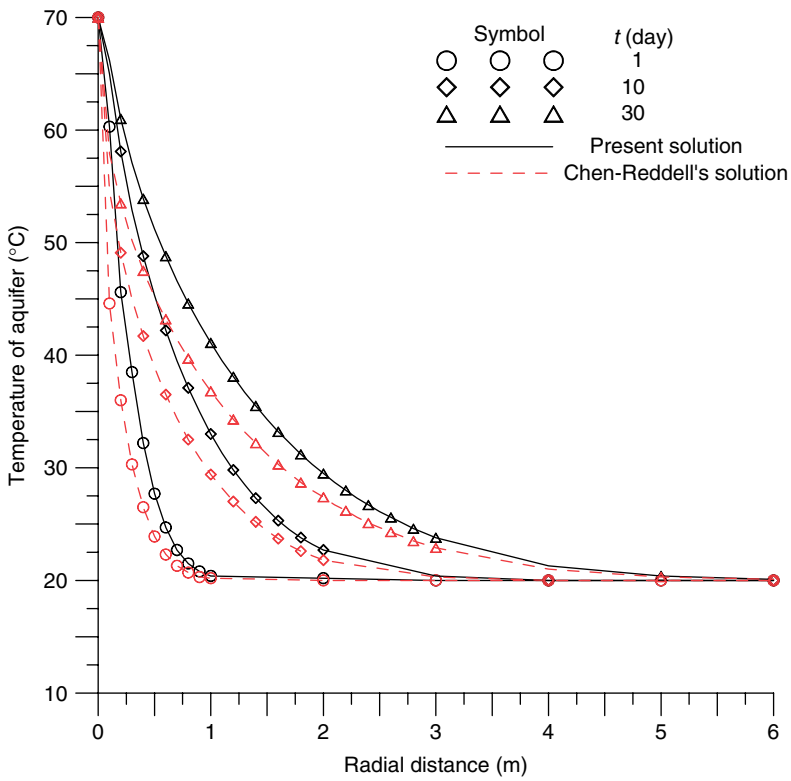

Figure 5. Comparisons of Chen–Reddell's solution and the present solution when $t = 1$, 10, or 30 days. The dotted and solid lines denote the semi-analytical results for aquifer temperature distribution estimated by Chen–Reddell's solution and the present solution, respectively

Table II. Parameters of the aquifer and the underlying and overlying rocks, which are of the same physical properties

Parameter name	Symbol	Value
Thickness of the aquifer	b_m	40 m
Thickness of the rocks	b_R	20 m
Volumetric thermal capacity of the aquifer	C_m	$2{\cdot}695 \times 10^6$ J/m$^3\cdot$°C
Volumetric thermal capacity of the rocks	C_R	$2{\cdot}65 \times 10^6$ J/m$^3\cdot$°C
Thermal conductivity of the aquifer	λ_m	2·4 W/m·°C
Thermal conductivity of the rocks	λ_R	2·0 W/m·°C
The aquifer porosity	n	1

CONCLUDING REMARKS

The following conclusions can be drawn from this study:

1. A mathematical model is developed to simulate the thermal distribution in an ATES system when hot water is injected into the confined aquifer. The Laplace domain solutions of dimensionless temperature are developed by Laplace transforms and their corresponding time-domain solutions are evaluated by the modified Crump method. In addition, the steady-state solutions for the confined aquifer and rocks are obtained by the final-value theorem.
2. The temperature in the aquifer and rocks after the injection of hot water increases with injection time and decreases with both the radial and vertical distances. The vertical thermal conduction in the rocks and the horizontal advection and thermal conduction in the aquifer have profound effects on temperature distributions in an ATES system. In addition, the aquifer temperature may be overestimated when ignoring the effect of thermal conductivity.
3. The present model is useful in estimating the effects of wellbore radius, injection temperature, thermal conductivity, rock thickness, and time on spatial and temporal temperature distributions of the aquifer and rocks in an ATES system. It is found that the aquifer temperature will be underestimated when ignoring the effect of wellbore radius. Accordingly, this model is also useful in designing an efficient ATES system, where the superfluous hot water is injected into a confined aquifer as disposal storage of waste heat energy.

NOTATION

b_i	thickness of the aquifer, m, $i = 1$, 2, or m
B_i	b_i/b_m, $i = 1$, 2; dimensionless thickness
C_m	$(\rho c)_m$, volumetric thermal capacity of the aquifer, J/m$^3\cdot$°C
C_1	$(\rho c)_1$, volumetric thermal capacity of the underlying rock, J/m$^3\cdot$°C
C_2	$(\rho c)_2$, volumetric thermal capacity of the overlying rock, J/m$^3\cdot$°C

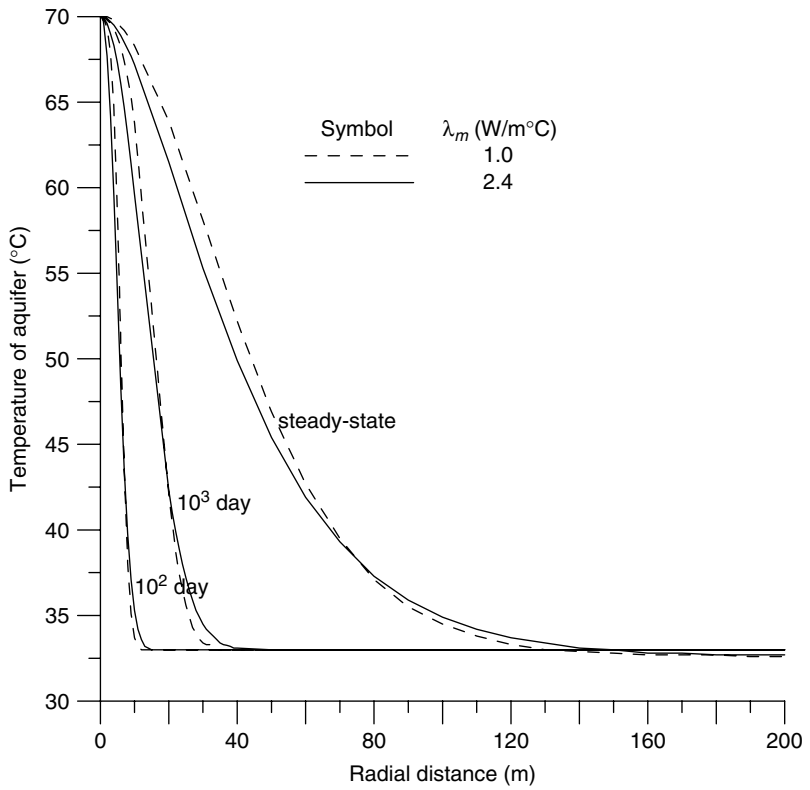

Figure 6. Temperature distribution of the aquifer for $\lambda_m = 1{\cdot}0$ and $2{\cdot}4$ W/m °C. The dotted and solid lines denote the temperature distribution of the aquifer for $\lambda_m = 1{\cdot}0$ and $2{\cdot}4$ W/m· °C, respectively

p	Laplace transform variable
q_i^2	$p/\alpha_{i\mathrm{D}}$, $i = 1$ and 2
Q	injection rate, m^3/s
r	radial distance from the centre of the injection well, m
r_0	the radius of the injection well, m
R	$2r/b_m$; dimensionless radial distance from the centre of the injection well
R_0	$2r_0/b_m$; dimensionless radius of the injection well
t	injection time, s
$T_m(r, t)$	temperature in the aquifer, °C
$T_1(r, z, t)$	temperature in the underlying rock, °C
$T_2(r, z, t)$	temperature in the overlying rock, °C
T_{m0}	initial temperature in the aquifer, °C
T_{10}	initial temperature in the underlying rock, °C
T_{20}	initial temperature in the overlying rock, °C
T_{in}	temperature of the injection water, °C
$T_{mD}(R, \tau)$	$\frac{T_m(r, t) - T_{m0}}{T_{in} - T_{m0}}$
$T_{1D}(R, Z_1, \tau)$	$\frac{T_1(r, z, t) - T_{m0}}{T_{in} - T_{m0}}$
T_{10D}	$\frac{T_{10} - T_{m0}}{T_{in} - T_{m0}}$
$T'_{1D}(R, Z_1, \tau)$	$T_{1D}(R, Z_1, \tau) - T_{10D}$
$T_{2D}(R, Z_2, \tau)$	$\frac{T_2(r, z, t) - T_{m0}}{T_{in} - T_{m0}}$
T_{20D}	$\frac{T_{20} - T_{m0}}{T_{in} - T_{m0}}$
$T'_{2D}(R, Z_2, \tau)$	$T_{2D}(R, Z_2, \tau) - T_{20D}$
$\overline{T}_{mD}(R_0, p)$	Dimensionless temperature of the aquifer in Laplace domain
$\overline{T}_{1D}(R, Z_1, p)$	Dimensionless temperature of the underlying rock in Laplace domain
$\overline{T}_{2D}(R, Z_2, p)$	Dimensionless temperature of the overlying rock in Laplace domain
v	$Q/2\pi rnb_m$; volumetric flux per unit area, m/s
w	$Q/4\pi nb_m\alpha_m$; dimensionless advection parameter
z	vertical distance along the injection well, m

Greek symbol

α_m	λ_m/C_m; thermal diffusivity of the aquifer, m^2/s
α_1	λ_1/C_1; thermal diffusivity of the underlying rock, m^2/s
α_2	λ_2/C_2; thermal diffusivity of the overlying rock, m^2/s
α_{1D}	$4\alpha_1/\alpha_m$; dimensionless thermal diffusivity of the underlying rock
α_{2D}	$4\alpha_2/\alpha_m$; dimensionless thermal diffusivity of the overlying rock
$A(p)$	$p + \lambda_{1D}q_1\coth(4q_1B_1) + \lambda_{2D}q_2\coth(4q_2B_2)$
$B(p)$	$-\lambda_{1D}q_1T_{10D}\coth(4q_1B_1) - \lambda_{2D}q_2T_{20D}\coth(4q_2B_2)$
λ_m	thermal conductivity of the aquifer, W/m· °C
λ_1	thermal conductivity of the underlying rock, W/m· °C

λ_2	thermal conductivity of the overlying rock, W/m·°C
λ_{1D}	λ_1/λ_m dimensionless thermal conductivity of the underlying rock
λ_{2D}	λ_2/λ_m dimensionless thermal conductivity of the underlying rock
τ	$4\alpha_m t/b_m^2$; dimensionless time from the start of the injecting water

ACKNOWLEDGEMENTS

Research leading to this article has been partially supported by the grants from Taiwan National Science Council under the contract numbers NSC96-2221-E-238-009 and NSC98-3114-E-007-015. The authors would like to thank the editor and three anonymous reviewers for their constructive comments and valuable suggestions.

APPENDIX A

Development of Equation (14)

Equations (1)–(12) can be arranged in dimensionless forms based on the normalized parameters given in Equation (13). The heat balance equation of the aquifer in dimensionless form is

$$\frac{\partial^2 T_{mD}(R,\tau)}{\partial R^2}+\left(\frac{1-2\ w}{R}\right)\frac{\partial T_{mD}(R,\tau)}{\partial R}+\lambda_{1D}\frac{\partial T_{1D}(R,Z_1,\tau)}{\partial Z_1}\bigg|+\lambda_{2D}\frac{\partial T_{2D}(R,Z_2,\tau)}{\partial Z_2}\bigg|_{Z_2=0}=\frac{\partial T_{mD}(R,\tau)}{\partial \tau} \tag{A1}$$

The initial condition is

$$T_{mD}(R,0)=0 \tag{A2}$$

and the boundary conditions are

$$T_{mD}(R_0,\tau)=1 \tag{A3}$$

and

$$T_{mD}(\infty,\tau)=0 \tag{A4}$$

The dimensionless heat conduction equation in the underlying rock can be written as

$$\frac{\partial^2 T'_{1D}(R,Z_1,\tau)}{\partial Z_1^2}=\frac{1}{\alpha_{1D}}\frac{\partial T'_{1D}(R,Z_1,\tau)}{\partial \tau},\ \alpha_{1D}=\frac{4\alpha_1}{\alpha_m} \tag{A5}$$

a where $Z_1=-4z/b_m$ and $0<Z_1<4B_1$.

The initial condition in dimensionless form is

$$T'_{1D}(R,Z_1,0)=0 \tag{A6}$$

and the boundary conditions in dimensionless form are

$$T'_{1D}(R,0,\tau)=T_{mD}(R,\tau)-T_{10D} \tag{A7}$$

and

$$T'_{1D}(R,4B_1,\tau)=0 \tag{A8}$$

The dimensionless heat conduction equation in the overlying rock can be written as

$$\frac{\partial^2 T'_{2D}(R,Z_2,\tau)}{\partial Z_2^2}=\frac{1}{\alpha_{2D}}\frac{\partial T'_{2D}(R,Z_2,\tau)}{\partial \tau},\ \alpha_{2D}=\frac{4\alpha_2}{\alpha_m} \tag{A9}$$

where $Z_2=4(z-b_m)/b_m$ and $0<Z_2<4B_2$.

The initial condition in dimensionless form is

$$T'_{2D}(R,Z_2,0)=0 \tag{A10}$$

The boundary conditions in dimensionless form are

$$T'_{2D}(R,0,\tau)=T_{mD}(R,\tau)-T_{20D} \tag{A11}$$

and

$$T'_{2D}(R,4B_2,\tau)=0 \tag{A12}$$

Taking Laplace transform of Equation (A1) yields

$$\frac{d^2\overline{T}_{mD}(R,p)}{dR^2}+\left(\frac{1-2\ w}{R}\right)\frac{d\overline{T}_{mD}(R,p)}{dR}+\lambda_{1D}\frac{d\overline{T}_{1D}(R,Z_1,p)}{dZ_1}\bigg|+\lambda_{2D}\frac{d\overline{T}_{2D}(R,Z_2,p)}{dZ_2}\bigg|_{Z_2=0}=p\overline{T}_{mD}(R,p) \tag{A13}$$

and the boundary conditions after taking Laplace transforms are

$$\overline{T}_{mD}(R_0,p)=\frac{1}{p} \tag{A14}$$

and

$$\overline{T}_{mD}(\infty,p)=0 \tag{A15}$$

The heat conduction equation of the underlying rock after taking Laplace transform becomes

$$\frac{d^2\overline{T}'_{1D}(R,Z_1,p)}{dZ_1^2}=q_1^2\overline{T}'_{1D}(R,Z_1,p),\ q_1^2=\frac{p}{\alpha_{1D}} \tag{A16}$$

and the related boundary conditions after taking Laplace transforms are

$$\overline{T}'_{1D}(R,0,p)=\overline{T}_{mD}(R,p)-\frac{T_{10D}}{p} \tag{A17}$$

and

$$\overline{T}'_{1D}(R,4B_1,p)=0 \tag{A18}$$

The heat conduction equation of the overlying rock after taking Laplace transform is

$$\frac{d^2\overline{T}'_{2D}(R,Z_2,p)}{dZ_2^2}=q_2^2\overline{T}'_{2D}(R,Z_2,p),\ q_2^2=\frac{p}{\alpha_{2D}} \tag{A19}$$

and the related boundary conditions after taking Laplace transforms are

$$\overline{T}'_{2D}(R,0,p)=\overline{T}_{mD}(R,p)-\frac{T_{20D}}{p} \tag{A20}$$

and

$$\overline{T}'_{2D}(R, 4B_2, p) = 0 \quad \text{(A21)}$$

Equations (A16) and (A19) are linear second-order homogeneous differential equations and the principle of superposition can be applied. That is

$$\overline{T}'_{1D}(R, Z_1, p) = A\overline{T}'^{(1)}_{1D} + B\overline{T}'^{(2)}_{1D} \quad \text{(A22)}$$

where A and B are the undetermined constants. Assume that the eigenfunction of $\overline{T}'_{1D}(R, Z_1, p)$ is represented by e^{mZ_1} with the eigenvalue m. One can substitute e^{mZ_1} into Equation (A16) and let their corresponding m's be equal to $\pm q_1$. Equation (A22) can therefore be obtained as

$$\overline{T}'_{1D}(R, Z_1, p) = A \cosh q_1 Z_1 + B \sinh q_1 Z_1 \quad \text{(A23)}$$

The undetermined constants can be determined after substituting Equation (A23) into Equations (A17) and (A18) and some algebraic manipulations as

$$A = \overline{T}_{mD}(R, p) - \frac{1}{p} T_{10D} \quad \text{(A24)}$$

and

$$B = \frac{-1}{\tanh(4q_1B_1)} \left[\overline{T}_{mD}(R, p) - \frac{1}{p} T_{10D} \right] \quad \text{(A25)}$$

Substituting Equations (A24) and (A25) into Equation (A23), the Laplace domain solution of the underlying rock can then be obtained as

$$\overline{T}'_{1D}(R, Z_1, p) = \frac{\sinh[q_1(4B_1 - Z_1)]}{\sinh(4q_1B_1)} \left(\overline{T}_{mD}(R, p) - \frac{T_{10D}}{p} \right) \quad \text{(A26)}$$

Based on $T'_{1D}(R, Z_1, \tau) = T_{1D}(R, Z_1, \tau) - T_{10D}$ in Equation (13), Equation (A26) can be rewritten as Equation (17).

Similarly, the Laplace domain solution of the overlying rock can be obtained from Equations (A19), (A20), and (A21) as

$$\overline{T}'_{2D}(R, Z_2, p) = \frac{\sinh[q_2(4B_2 - Z_2)]}{\sinh(4q_2B_2)} \left(\overline{T}_{mD}(R, p) - \frac{T_{20D}}{p} \right) \quad \text{(A27)}$$

This equation can be rewritten in dimensionless form as Equation (18) based on Equation (13).

Substituting Equations (17) and (18) into Equation (A13), one obtains

$$\frac{d^2\overline{T}_{mD}(R, p)}{dR^2} + \left(\frac{1 - 2\,w}{R} \right) \frac{d\overline{T}_{mD}(R, p)}{dR} - q_1\lambda_{1D} \left[\frac{(\overline{T}_{mD}(R, p) - T_{10D}/p)}{\tanh(4q_1B_1)} \right] - q_2\lambda_{2D} \left[\frac{(\overline{T}_{mD}(R, p) - T_{20D}/p)}{\tanh(4q_2B_2)} \right] = p\overline{T}_{mD}(R, p) \quad \text{(A28)}$$

Furthermore, based on Equations (15) and (16), Equation (A28) can be expressed as

$$\frac{d^2\overline{T}_{mD}(R, p)}{dR^2} + \left(\frac{1 - 2\,w}{R} \right) \frac{d\overline{T}_{mD}(R, p)}{dR} - A(p)\overline{T}_{mD}(R, p) = \frac{1}{p} B(p) \quad \text{(A29)}$$

Equation (A29) is a linear second-order differential equation and can be solved by applying the superposition principle. The solution of Equation (A29) in Laplace domain includes the general solution, $\overline{T}^h_{mD}$, and the particular solution, $\overline{T}^p_{mD}$. As such

$$\overline{T}_{mD} = \overline{T}^h_{mD} + \overline{T}^p_{mD} \quad \text{(A30)}$$

The homogeneous equation of Equation (A29) is a special form of Bessel equation and its solution can be expressed as

$$\overline{T}^h_{mD} = R^w \left[CI_w(\sqrt{A(p)}R) + DK_w(\sqrt{A(p)}R) \right] \quad \text{(A31)}$$

The non-homogeneous equation of Equation (A29) can be solved by the method of the undetermined constants and its particular solution is

$$\overline{T}^p_{mD} = -\frac{B(p)}{pA(p)} \quad \text{(A32)}$$

Based on the superposition principle, the Laplace domain solution can then be obtained as

$$\overline{T}_{mD} = R^w[CI_w(\sqrt{A(p)}R) + DK_w(\sqrt{A(p)}R)] - \frac{B(p)}{pA(p)} \quad \text{(A33)}$$

Substituting Equation (A33) into Equations (A14) and (A15), the undetermined constants can be determined as

$$C = 0 \quad \text{(A34)}$$

and

$$D = \frac{1}{p} \left(\frac{1}{R_0} \right)^w \left[\frac{1}{K_w(\sqrt{A(p)}R_0)} \right] \left[1 + \frac{B(p)}{A(p)} \right] \quad \text{(A35)}$$

Then, Equation (14) can be obtained by substituting the constants of Equations (A34) and (A35) into Equation (A33).

APPENDIX B

Derivation of Equation (24)

Equation (22) is developed under the conditions that the well radius is neglected (i.e. $r_0 = 0$) and the underlying and overlying rocks are of the same initial temperature and thickness (Chen and Reddell, 1983). Then, Equation (22) can be reduced to

$$\overline{T}^*_{mD}(R, p) = \lim_{R_0 \to 0} \frac{1}{p} \left(\frac{R}{R_0} \right)^w \left[\frac{K_w(\sqrt{A^*(p)}R)}{K_w(\sqrt{A^*(p)}R_0)} \right] \quad \text{(B1)}$$

Using the ascending series for $I_w(R_0)$ as $R_0 \to 0$, $K_w(R_0)$ becomes (Abramowitz and Stegun, 1964, p. 375)

$$K_w(R_0) = \frac{\pi}{2}\frac{I_{-w}(R_0) - I_w(R_0)}{\sin(w\pi)} \tag{B2}$$

with

$$I_w(R_0) = \left(\frac{R_0}{2}\right)^w \sum_{k=0}^{\infty} \frac{\left(\frac{1}{4}R_0^2\right)^k}{k!\Gamma(w+k+1)} \tag{B3}$$

where $\Gamma(\cdot)$ is the gamma function. Substituting Equation (B2) into Equation (B1), one can obtain

$$\overline{T}^*_{mD}(R, p) = \frac{R^w K_w(\sqrt{A^*(p)}R)}{p} \left[\frac{2^{1-w}\sqrt{A^*(p)}^w \sin(w\pi)\Gamma(1-w)}{\pi}\right] \tag{B4}$$

Abramowitz and Stegun (1964, p. 256) provides

$$\Gamma(u)\Gamma(1-u) = \pi\csc(u\pi) \quad (0 < \Re u < 1) \tag{B5}$$

Substituting Equation (B5) into Equation (B4) results in Equation (24).

APPENDIX C

Derivation of Equation (25)

A steady-state solution can be obtained from the transient solution by applying the final-value theorem (Yeh and Wang, 2007) as

$$T_{mD}(R, \infty) = \lim_{p\to 0} p\overline{T}_{mD}(R, p) \tag{C1}$$

Accordingly, substituting Equation (14) into Equation (C1) yields

$$T_{mD}(R, \infty) = \lim_{p\to 0}\left\{\left(\frac{R}{R_0}\right)^w \left[\frac{K_w(\sqrt{A(p)}R)}{K_w(\sqrt{A(p)}R_0)}\right]\left[1 + \frac{B(p)}{A(p)}\right] - \frac{B(p)}{A(p)}\right\} \tag{C2}$$

Abramowitz and Stegun (1964, p. 85) gives

$$\coth(u) = \frac{1}{u} + \frac{u}{3} - \frac{u^3}{45} + \frac{2}{945}u^5 - \cdots + \frac{2^{2n}B_{2n}}{(2n)!}u^{2n-1} + \cdots, \quad |u| < \pi \tag{C3}$$

where B_n is the nth Bernoulli number. With $x = (4q_1B_1)$ and $y = (4q_2B_2)$, using Equation (C3) leads Equations (15) and (16) respectively to

$$A(p) = p + \lambda_{1D}q_1\left[\frac{1}{x} + \frac{x}{3} - \frac{x^3}{45} + \frac{2}{945}x^5 - \cdots + \frac{2^{2n}B_{2n}}{(2n)!}x^{2n-1} + \cdots\right] + \lambda_{2D}q_2\left[\frac{1}{y} + \frac{y}{3} - \frac{y^3}{45} + \frac{2}{945}y^5 - \cdots + \frac{2^{2n}B_{2n}}{(2n)!}y^{2n-1} + \cdots\right] \tag{C4}$$

and

$$B(p) = -\lambda_{1D}q_1T_{1D}\left[\frac{1}{x} + \frac{x}{3} - \frac{x^3}{45} + \frac{2}{945}x^5 - \cdots + \frac{2^{2n}B_{2n}}{(2n)!}x^{2n-1} + \cdots\right] - \lambda_{2D}q_2T_{2D}\left[\frac{1}{y} + \frac{y}{3} - \frac{y^3}{45} + \frac{2}{945}y^5 - \cdots + \frac{2^{2n}B_{2n}}{(2n)!}y^{2n-1} + \cdots\right] \tag{C5}$$

When $p \to 0$, Equations (C4) and (C5), respectively, reduce to

$$A(0) = \frac{1}{4}\left(\frac{\lambda_{1D}}{B_1} + \frac{\lambda_{2D}}{B_2}\right) \tag{C6}$$

and

$$B(0) = -\frac{1}{4}\left(\frac{\lambda_{1D}T_{1D}}{B_1} + \frac{\lambda_{2D}T_{2D}}{B_2}\right) \tag{C7}$$

Equation (25) can then be obtained after substituting Equations (C6) and (C7) into Equation (C2).

REFERENCES

Abramowitz M, Stegun IA. 1964. *Handbook of Mathematical Functions With Formulas, Graphs and Mathematical Tables*. National Bureau of Standards: Washington, DC.

Avdonin NA. 1964. Some formulas for calculating the temperature field of a stratum subjected to thermal injection. *Neft'i Gaz* **7**(3): 37–41.

Bödvarsson GS, Tsang CF. 1982. Injection and thermal breakthrough in fractured geothermal reservoirs. *Journal of Geophysical Research* **87**(B2): 1031–1048.

Bödvarsson GS, Benson SM, Witherspoon PA. 1982. Theory of the development of geothermal systems charged by vertical faults. *Journal of Geophysical Research* **87**: 9317–9328.

Brookfield AE, Studicky EA, Park Y-J, Conant B, Jr. 2009. Thermal transport modeling in a fully integrated surface/subsurface framework. *Hydrological Processes* **23**: 2150–2164.

Carotenuto A, Casarosa C, Martorano L. 1999. The geothermal convector: experimental and numerical results. *Applied Thermal Engineering* **19**: 349–374.

Chen CS, Reddell DL. 1983. Temperature distribution around a well during thermal injection and a graphical technique for evaluating aquifer thermal properties. *Water Resources Research* **19**(2): 351–363.

Chevalier S, Banton O. 1999a. Modeling of heat transfer with the random walk method: Part 1. Application to thermal energy storage in porous aquifers. *Journal of Hydrology* **222**: 129–139.

Chevalier S, Banton O. 1999b. Modeling of heat transfer with the random walk method: Part 2. Application to thermal energy storage in fractured aquifers. *Journal of Hydrology* **222**: 140–151.

Crump KS. 1976. Numerical inversion of Laplace transforms using a Fourier series approximation. *Journal of the Association for Computing Machinery* **23**(1): 89–96.

de Hoog FR, Knight JH, Stokes AN. 1982. An improved method for numerical inversion of Laplace transforms, Society for Industrial and Applied Mathematics. *Journal on Scientific Computing* **3**(3): 357–366.

Doughty C, Hellström G, Tsang CF, Claesson J. 1982. A dimensionless parameters approach to the thermal behavior of an aquifer thermal energy storage system. *Water Resources Research* **18**(3): 571–587.

Golden Software. 1999. *Surfer*, version 7.00. Golden Software, Golden, CO.

IMSL. 2003. *IMSL Fortran Library User's Guide Math/Library Volume 2 of 2*, version 5.0. Visual Numerics: Houston.

Molson JW, Frind EO, Palmer CD. 1992. Thermal energy storage in an unconfined aquifer: 2. Model development, validation, and application. *Water Resources Research* **28**(10): 2857–2867.

Molz FJ, Warman JC, Jones TE. 1978. Aquifer storage of heated water: 1. A field experiment. *Ground Water* **16**(4): 234–241.

Molz FJ, Parr AD, Anderson PF, Lucido VD, Warman JC. 1979. Thermal energy storage in a confined aquifer: experimental results. *Water Resources Research* **15**(6): 1509–1514.

Mongelli F, Pagliarulo P. 1997. Influence of water recharge on heat transfer in a semi-infinite aquifer. *Geothermics* **26**(3): 365–378.

Nagano K, Mochida T, Ochifuji K. 2002. Influence of natural convection on forced horizontal flow in saturated porous media for aquifer thermal energy storage. *Applied Thermal Engineering* **22**: 1299–1311.

Özisik MN. 1993. *Heat conduction*, 2nd edn. John Wiley & Sons Inc: New York; 25.

Paksoy HO, Gurbuz Z, Turgut B, Dikici D, Evliya H. 2004. Aquifer thermal storage (ATES) for air-conditioning of a supermarket in Turkey. *Renewable Energy* **29**: 1991–1996.

Palmer CD, Blowes DW, Frind EO, Molson JW. 1992. Thermal energy storage in an unconfined aquifer: 1. Field injection experiment. *Water Resources Research* **28**(10): 2845–2856.

Rubinstein LI. 1959. The total heat loss in injection of a hot liquid into a stratum. *Neft'i Gaz* **2**(9): 41–48.

Rubinstein LI. 1962. An asymptotic solution of an axially symmetric contact problem in thermal convection for higher values of the convection parameter. *Dan SSSR* **146**(5): 1043–1046.

Sauty JP, Gringarten AC, Menjoz A, Landel PA. 1982. Sensible energy storage in aquifers 1. Theoretical study. *Water Resources Research* **18**(2): 245–252.

Shanks D. 1955. Non-linear transformations of divergent and slowly convergent sequences. *Journal of Mathematical Physics* **34**: 1–42.

Spiegel MR. 1965. *Theory and Problems of Laplace Transforms*. Schaum: New York.

Stopa J, Wojnarowski P. 2006. Analytical model of cold water front movement in a geothermal reservoir. *Geothermics* **35**: 59–69.

Thomas GW. 1967. Approximate methods for calculating the temperature distribution during hot fluid injection. *Journal of Canadian Petroleum Technology* **6**(4): 123–129.

Tsang CF, Buscheck T, Doughty C. 1981. Aquifer thermal energy storage: a numerical simulation of Auburn University field experiments. *Water Resources Research* **17**(3): 647–658.

Yang SY, Yeh HD. 2008. An analytical solution for modeling thermal energy transfer in a confined aquifer system. *Hydrogeology Journal* **16**: 1507–1515.

Yang SY, Yeh HD. 2009a. Modeling heat extraction from hot dry rock in a multiple well system. *Applied Thermal Engineering* **29**(8–9): 1676–1681.

Yang SY, Yeh HD. 2009b. Modeling heat transfer in a deep hypothetical geological repository for a spent nuclear fuel. *Journal of hazardous material* **169**: 108–112.

Yeh HD, Wang CT. 2007. Large-time solutions for groundwater flow problems using the relationship of small p versus large t. *Water Resources Research* **43**(6): W06502, 1–6.

Yeh HD, Yang SY. 2006. A novel analytical solution for a slug test conducted in a well with a finite-thickness skin. *Advances in Water Resources* **29**(10): 1479–1489.

Ziagos JP, Blackwell DD. 1986. A model for the transient temperature effects of horizontal fluid flow in geothermal systems. *Journal of Volcanology and Geothermal Research* **27**: 371–397.

